Hyperfine coupling constants on inner-sphere water molecules of Gd^{III}-based MRI contrast agents[i]

David Esteban-Gómez[a], Andrés de Blas[a], Teresa Rodríguez-Blas[a], Lothar Helm[b] and Carlos Platas-Iglesias[a*]

[a] Departamento de Química Fundamental, Universidade da Coruña, Campus da Zapateira-Rúa da Fraga 10, 15008A Coruña (Spain)

[b] Laboratoire de Chimie Inorganique et Bioinorganique, Ecole Polytechnique Fédérale de Lausanne, EPFL-BCH, CH-1015 Lausanne (Switzerland)

ChemPhysChem, volume 13, issue 16, pages 3640–3650, 12 November 2012
Received 24 May 2012, version of record online 27 August 2012, issue online 02 November 2012

This is the peer reviewed version of the following article:

Esteban-Gómez, D. , de Blas, A. , Rodríguez-Blas, T. , Helm, L. and Platas-Iglesias, C. (2012), Hyperfine Coupling Constants on Inner-Sphere Water Molecules of Gd^{III}-Based MRI Contrast Agents. *ChemPhysChem*, 13: 3640-3650

which has been published in final form at https://doi.org/10.1002/cphc.201200417. This article may be used for non-commercial purposes in accordance with Wiley Terms and Conditions for Use of Self-Archived Versions.

Abstract

Herein we present a theoretical investigation of the hyperfine coupling constants (HFCCs) on the inner-sphere water molecules of $[Gd(H_2O)_8]^{3+}$ and different Gd^{III}-based magnetic resonance imaging contrast agents such as $[Gd(DOTA)(H_2O)]^-$, $[Gd(DTPA)(H_2O)]^{2-}$, [Gd(DTPA-BMA)(H_2O)] and [Gd(HP-DO3A)(H_2O)]. DFT calculations performed on the $[Gd(H_2O)_8]^{3+}$ model system show that both hybrid-GGA functionals (BH&HLYP, B3PW91 and PBE1PBE) and the hybrid meta-GGA functional TPSSh provide ^{17}O HFCCs in close agreement with the experimental data. The use of all-electron relativistic approaches based on the DKH2 approximation and the use of relativistic effective core potentials (RECP) provide results of essentially the same quality. The accurate calculation of HFCCs on the $[Gd(DOTA)(H_2O)]^-$, $[Gd(DTPA)(H_2O)]^{2-}$, [Gd(DTPA-BMA)(H_2O)] and [Gd(HP-DO3A)(H_2O)] complexes requires an adequate description of solvent effects. This was achieved by using a mixed cluster/continuum approach that includes explicitly two second-sphere water molecules. The calculated isotropic ^{17}O HFCCs (A_{iso}) fall within the range 0.40–0.56 MHz, and show deviations from the corresponding experimental values typically lower than 0.05 MHz. The A_{iso} values are significantly affected by the distance between the oxygen atom of the coordinated water molecule and the Gd^{III} ion, as well as by the orientation of the water molecule plane with respect to the Gd-O vector. ^1H HFCCs of coordinated water molecules and ^{17}O HFCCs of second-sphere water molecules take values close to zero.

Keywords: density functional calculations; f-group elements; hyperfine couplings; lanthanides; MRI contrast agents

* carlos.platas.iglesias@udc.es

Introduction

Gadolinium(III) complexes with poly(aminocarboxylate) ligands have attracted considerable interest during the last two decades since they are commonly used as contrast agents (CAs) in magnetic resonance imaging (MRI).[1,2] CAs are paramagnetic probes that enhance the image contrast by preferentially influencing the longitudinal and/or transverse relaxation times of water molecules in the vicinity of the complex. Commercially available Gd^{III}-based contrast agents contain one water molecule coordinated to the metal ion that exchanges rapidly with the bulk water. The efficiency of a CA is evaluated in vitro in terms of its relaxivity, which is defined as the longitudinal relaxation rate enhancement of water proton nuclei per mM concentration of gadolinium ions. The observed relaxivity is accounted for by the presence of two different contributions: outer-sphere relaxation, which is the result of free diffusion of water molecules in the vicinity of the metal center, and inner-sphere relaxation, which is the result of the exchange between the coordinated water molecule(s) and the bulk water. The inner-sphere contribution to relaxivity is proportional to the number of water molecules coordinated to the metal ion (q). The ^{1}H longitudinal relaxation rate of the inner-sphere water molecules is dominated by the dipolar interaction, which is proportional to $1/r^6$, where r is the distance between the metal ion and the inner-sphere water proton nuclei. Additionally, the inner-sphere contribution depends on four correlation times: the residence time of a water proton in the inner coordination sphere (τ_m), the rotational correlation time of the Gd···H vector (τ_R), and the longitudinal and transverse electronic relaxation times of the metal ion (T_{1e} and T_{2e}).[3] These correlation times show temperature dependence, and as a result the inner-sphere contribution to relaxivity depends on a relatively large number of parameters. Besides this, the outer-sphere contribution depends on the distance of closest approach of an outer-sphere water molecule to Gd^{III} and the diffusion coefficient for the translational diffusion of a water molecule away from the Gd^{III} chelate, which also varies with temperature.[4] Thus, there are a large number of parameters determining the relaxivity of a given compound, and it is difficult to determine them from relaxivity measurements without obtaining independent information of at least some of the most important parameters.[5]

Variable-temperature ^{17}O NMR measurements of chemical shifts and longitudinal and transverse relaxation rates constitute a valuable tool to investigate the parameters influencing relaxivity in MRI CAs.[1] ^{17}O NMR data provide information on the water exchange kinetics of the complex as well as on the rotational correlation time.[6] A combined analysis of the ^{1}H relaxivity and ^{17}O NMR data has been applied successfully to evaluate the parameters governing relaxivity in many Gd^{III} complexes.[7] Both the ^{17}O NMR chemical shifts and relaxation rates depend on the hyperfine coupling constant $A/\hbar$ between the electron spin of the metal ion and the ^{17}O nuclear spin. For the Gd^{III} aqua-ion $[Gd(H_2O)_8]^{3+}$ $A/\hbar$ was determined to be 5.3×10^6 rad s^{-1};[5] the values measured for many small Gd^{III} chelates fall within a relatively narrow range of $3.9\pm0.3\times10^6$ rad s^{-1}.[5,7,8] Some examples exist in the literature where significantly lower hyperfine coupling constants have been reported.[9] These examples include $[Gd(BPEDA)(H_2O)]^-$ and [Gd(HP-DO3A)(H_2O)], for which $A/\hbar$ values of 2.3×10^6 rad s^{-1} and 2.9×10^6 rad s^{-1} have been determined (Scheme **1**).[10,11] However, these results should be taken with care, since unusually low fitted $A/\hbar$ values could also be the result of a hydration number lower than expected, for instance due to the presence in solution of an equilibrium between complex species with different hydration numbers. Indeed, different examples of small Gd^{III} complexes that present hydration equilibria in solution have been reported in the literature.[12,13]

Although high-level correlated wave-function-based ab initio computational methods have successfully been applied to calculate hyperfine coupling constants in small organic radicals,[14] the scaling behaviour of these methods with system size prevent their application to larger systems with the currently available computational resources. In the last decade, methods based on density functional theory (DFT) have become an attractive tool for the calculation of hyperfine coupling constants (HFCCs) due to the high accuracy that can be achieved at relatively low computational cost. Indeed, DFT calculations have been shown to provide accurate HFCCs for both small organic radicals[15] and transition metal complexes.[16] Yazyev et al.

investigated the hyperfine interactions of ^{1}H and ^{17}O nuclei of inner-sphere water molecules in $[Gd(H_2O)_8]^{3+}$ and $[Gd(DOTA)(H_2O)]^{-}$ complexes.[17] The approach used to calculate the hyperfine interactions involved either classical or Car–Parrinello molecular dynamics (MD) simulations. From the trajectories of these simulations clusters of molecules were extracted, and then investigated by using DFT calculations, which provided ^{17}O hyperfine coupling constants in good agreement with the experimental values.[18] The main drawback of this approach is that Gd^{III} complexes with relevance in MRI can be hardly handled with Car–Parrinello MD calculations due to the excessive computational cost, and thus HFCCs must be calculated on clusters taken from classical MD simulations, which might be problematic due to the lack of parametrization of many Gd^{III} complexes in commonly available force fields. On the other hand, MD simulations have the advantage that allows one to perform a meaningful sampling of different configurations, as the observed HFCC corresponds to the mean value of all configurations in solution.

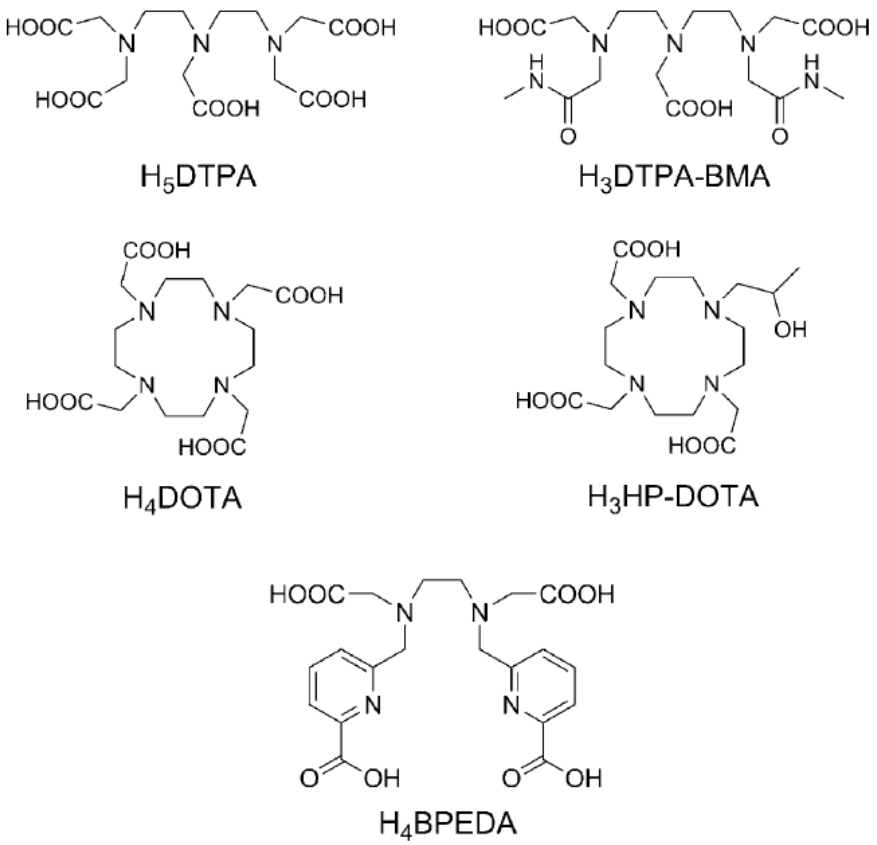

Scheme 1. Ligands discussed herein.

The aim of this work is to develop a simple methodology based on DFT for the calculation of ^{17}O hyperfine coupling constants of coordinated water molecules in Gd^{III} complexes, and to investigate the reasons for the particularly low hyperfine coupling constants determined experimentally for some of them. For this purpose we have selected different Gd^{III} complexes such as $[Gd(DOTA)(H_2O)]^{-}$ (gadoterate meglumine, Dotarem; Guerbet, Aulnaysous-Bois, France), $[Gd(DTPA)(H_2O)]^{2-}$ (gadopentetate dimeglumine, Magnevist; Schering, Berlin, Germany), $[Gd(DTPA\text{-}BMA)(H_2O)]$ (gadodiamide, Omniscam; Nycomed, Oslo, Norway) and $[Gd(HP\text{-}DO3A)(H_2O)]$ (Gadoteridol, ProHance; Bracco, Milan, Italy) currently used in clinical practice as MRI CAs (Scheme **1**). Additionally, we have performed calculations on $[Gd(BPEDA)(H_2O)]^{-}$ as a representative example of a complex for which a low $A/\hbar$ value has been reported.[10] The fitting of the

experimental ^{17}O NMR data often requires one to consider an outer-sphere contribution to the observed chemical shifts. Herein we present a set of calculations performed on molecular clusters, explicitly including second-sphere water molecules, that allows one to obtain information about the scalar outer-sphere contribution to the ^{17}O NMR chemical shifts. Finally, we have also calculated ^{1}H hyperfine coupling constants to confirm that the scalar mechanism to the proton relaxation enhancement can be safely neglected.

Theory

The hyperfine coupling tensor for the nucleus *N* consists of three contributions, which are the isotropic Fermi contact (FC) and the anisotropic spin–dipolar contributions and the spin–orbit contribution. Herein we focus on the calculation of isotropic FC contribution (A_{iso}), which is given by Equation **(1)**:[19]

$$A_{\mathrm{iso}}(N) = \frac{4\pi}{3S}\beta_{\mathrm{e}}\beta_{\mathrm{N}}g_{\mathrm{e}}g_{\mathrm{N}}\rho^{\alpha-\beta}(R_{\mathrm{N}}) \quad (1)$$

where β_N and β_e are the nuclear and Bohr magnetons, respectively, g_N and g_e are nuclear and free-electron *g* values, *S* is the total electron spin of the system, and $\rho^{\alpha-\beta}(R_N)$ represents the difference between majority spin (α) and minority spin (β) densities at the position of the nucleus *N*. Thus, A_{iso} is proportional to the value of the spin density at the position of nucleus *N*, which may be transmitted directly through the bonds by spin delocalization and/or by spin polarization.

Experimental values of isotropic ^{17}O HFCCs have been determined for many Gd^{III} chelates from ^{17}O NMR chemical shifts and as absolute values from transverse relaxation rates. The reduced transverse relaxation rates and chemical shifts, $1/T_{2r}$ and ω_r, observed on bulk water nuclei may be written as in Equations **(2)**–**(3)**,[20] where $1/T_{2m}$ is the relaxation rate of the bound water, τ_m is the residence time of water molecules in the inner sphere, $\Delta\omega_m$ is the chemical shift difference between bound and bulk water, and $\Delta\omega_{OS}$ is the outer sphere contribution to the chemical shift.

$$\frac{1}{T_{2\mathrm{r}}} = \frac{1}{\tau_{\mathrm{m}}}\frac{T_{2\mathrm{m}}^{-2}+\tau_{\mathrm{m}}^{-1}T_{2\mathrm{m}}^{-1}+\Delta\omega_{\mathrm{m}}^{2}}{\left(\tau_{\mathrm{m}}^{-1}+T_{2\mathrm{m}}^{-1}\right)^{2}+\Delta\omega_{\mathrm{m}}^{2}} \quad (2)$$

$$\Delta\omega_{\mathrm{r}} = \frac{\Delta\omega_{\mathrm{m}}}{\left(1+\tau_{\mathrm{m}}T_{2\mathrm{m}}^{-1}\right)^{2}+\tau_{\mathrm{m}}^{2}\Delta\omega_{\mathrm{m}}^{2}} + \Delta\omega_{\mathrm{os}} \quad (3)$$

$\Delta\omega_m$ is governed by the hyperfine or scalar interaction according to Equation **(4)**, where *B* represents the magnetic field, *S* is the electron spin and g_L is the isotropic Landé *g* factor.[21]

$$\Delta\omega_{\mathrm{m}} = \frac{g_{\mathrm{L}}\mu_{\mathrm{B}}S(S+1)}{3k_{\mathrm{B}}T}\frac{A}{\hbar} \quad (4)$$

It must be pointed out that for f^7 ions such as Gd^{III}, the ligand field splitting is zero under first-order conditions, and therefore no pseudocontact contribution to the hyperfine shifts is expected. However, higher-order effects may provoke the splitting of the J=7/2 level, and therefore a small pseudocontact shift. It has been estimated that such high-order effects may result in shifts of ~0.25 ppm,[22] while Equation (4) predicts a ^{17}O contact shift of 2545 ppm at 298 K for a typical $A/\hbar$ value of 3.9×10^6 rad s^{-1}. Thus, pseudocontact contributions to the ^{17}O NMR shifts of coordinated water molecules in Gd^{III} complexes can be safely neglected. It has been suggested that the outer-sphere contribution to $\Delta\omega_r$ may be represented by an empirical constant C_{OS} as given by Equation **(5)**:[5]

$$\Delta\omega_{OS} = C_{OS}\Delta\omega_m \quad (5)$$

The transverse ^{17}O NMR relaxation of bound water molecules is dominated by the scalar contribution, $1/T_{2sc}$, as given in Equation **(6)**:[23]

$$\frac{1}{T_{2m}} \cong \frac{1}{T_{2sc}} = \frac{S(S+1)}{3}\left(\frac{A}{\hbar}\right)^2 \tau_{s1} \quad (6)$$

where $1/\tau_{s1}$ is the sum of the exchange rate constant $k_{ex}=1/\tau_m$ and the electron spin relaxation rate $1/T_{1e}$. Thus, both the ^{17}O NMR chemical shifts and transverse relaxation rates depend on the HFCC $A/\hbar$. In Equations (4) and (6) $A/\hbar$ is expressed in rad s^{-1}, and therefore equals $2\pi\cdot A_{iso}$ as defined in Equation (1).

Computational methods

All calculations presented herein were performed employing the Gaussian 09 package (Revision B.01).[24] An important issue for the adequate computational description of Ln^{III} complexes is the treatment of relativistic effects.[25] In general, two different approaches have been developed to handle relativistic effects in systems containing heavy elements, namely the use of all-electron relativistic approaches such as the DKH2 and ZORA approximations,[26] and the use of relativistic effective core potentials (RECP). The most widely used approximation to treat relativistic effects in Ln^{III} complexes is the RECP approach, in which only the chemically relevant valence electrons are treated explicitly and relativistic effects are implicitly accounted for by a proper adjustment of free parameters in the valence model Hamiltonian.[27] In the present work we employed the energy-consistent quasirelativistic ECPs and associated basis sets of Dolg and coworkers,[28,29] for which two different core definitions have been developed: "large-core" (LC), in which the 4f electrons are included in the core, and "small-core" (SC), which treats the four-, five- and six-shell electrons explicitly. The LCRECP includes 46+$4f^7$ electrons in the core for Gd^{III}, while the outermost eight electrons are treated explicitly with a [5s4p3d]-GTO valence basis set. For the SCRECP, which includes 28 electrons in the core, we selected the associated ECP28MWB_GUESS basis set.[30] Full geometry optimizations of the $[Gd(BPEDA)(H_2O)]^-\cdot x\,H_2O$, $[Gd(DOTA)(H_2O)]^-\cdot x\,H_2O$, $[Gd(DTPA)(H_2O)]^{2-}\cdot x\,H_2O$, $[Gd(DTPA\text{-}BMA)(H_2O)]\cdot x\,H_2O$ and $[Gd(HP\text{-}DO3A)(H_2O)]\cdot x\,H_2O$ systems (x=0, 1, or 2) were performed in aqueous solution employing DFT within the hybrid meta generalized gradient approximation (hybrid *meta*-GGA), with the TPSSh exchange–correlation functional.[31] Input geometries of the $[Gd(BPEDA)(H_2O)]^-$ and $[Gd(DOTA)(H_2O)]^-$ systems for geometry optimization were taken from previous computational

studies.[10,32] For the $DOTA^{4-}$ complex, which is known to exist in solution as a mixture of square antiprismatic (SAP) and twisted-square antiprismatic (TSAP) isomers, we performed our calculations for both isomers.[33] The input geometry of [Gd(HP-DO3A)(H_2O)] was constructed from that of the $DOTA^{4-}$ analogue, and only the SAP isomer was considered. The starting geometry of $[Gd(DTPA)(H_2O)]^{2-}$ was taken from the X-ray structure of the MS-325 analogue,[34] while that of [Gd(DTPA-BMA)(H_2O)] was constructed from the optimized geometry of the DTPA analogue by adding the methylamide groups. Thus, only one of the four diasteroisomers of the complex observed in aqueous solution has been investigated (the *cis* isomer).[35]

For geometry optimization purposes we used the LCRECP for Gd, while the standard 6-31G(d) basis set was used for C, H, N and O atoms. No symmetry constraints have been imposed during the optimizations. The use of LCRECPs requires a separate potential for each oxidation state or 4f subconfiguration, which precludes the modeling of f–f centered processes and the treatment of spin–orbit coupling. However, this approach avoids many difficulties associated to the computational treatment of open-shell systems, and despite their approximate nature, it is an efficient computational tool that has proven to give good results in studies that focus on the structural features or the estimates of relative energies for Ln^{III} complexes at both the HF and DFT level.[36] The stationary points found on the potential energy surfaces as a result of the geometry optimizations have been tested to represent energy minima rather than saddle points via frequency analysis.

Isotropic ^{17}O HFCCs in the $[Gd(H_2O)_8]^{3+}$ model system were calculated in aqueous solution with unrestricted DFT methods by employing different functionals within the LSDA approximation (SVWN[37,38] and SPL[39]), GGA (BLYP,[40,41] G96LYP,[41,42,43] mPWLYP[41,44]), *meta*-GGA (BB95,[40,45] TPSS[31]), hybrid-GGA (B3LYP,[41,46] BH&HLYP,[47] PBE1PBE1,[48] and B3PW91[46,49]) and hybrid *meta*-GGA (TPSSh[31]). The geometry of the $[Gd(H_2O)_8]^{3+}$ system is the same as described in a previous paper,[50] obtained from geometry optimizations in aqueous solution (PCM model) at the B3LYP/LCRECP/6-31+G(d) level. The coordination environment around the metal ion in $[Gd(H_2O)_8]^{3+}$ corresponds to a slightly distorted square antiprismatic geometry of D_{4d} symmetry with a Gd—O distance of 2.433 Å. Both the mean Gd—O distance and the metal coordination environment are in good agreement with previous theoretical investigations.[51] For HFCC calculation purposes we used both the SCRECP approach and the all-electron second-order Douglas–Kroll–Hess (DKH2) method as implemented in Gaussian 09,[52] which employs a Gaussian nuclear model. For DKH2 calculations, the all-electron scalar relativistic basis set of Pantazis and Neese was used for Gd.[53] DFT investigations of HFCCs require the use of specifically developed basis sets with extra flexibility in the core region.[54] Thus, for the description of water molecules of $[Gd(H_2O)_8]^{3+}$ in both DKH2 and SCRECP calculations we used the EPR-II and EPR-III basis sets of Barone,[55] which were optimized for the computation of HFCCs by DFT methods. EPR-II is a double-zeta basis set with a single set of polarization functions and an enhanced s part, while EPR-III is a triple-zeta basis set including diffuse functions, double d polarizations and a single set of f-polarization functions. Both basis sets contain an improved s part to better describe the nuclear region. The isotropic ^{17}O and ^{1}H HFCCs in $[Gd(BPEDA)(H_2O)]^{-}\cdot x\,H_2O$, $[Gd(DOTA)(H_2O)]^{-}\cdot x\,H_2O$, $[Gd(DTPA)(H_2O)]^{2-}\cdot x\,H_2O$, [Gd(DTPA-BMA)($H_2O$)]$\cdot x\,H_2O$ and [Gd(HP-DO3A)(H_2O)]$\cdot x\,H_2O$ (x=0, 1 or 2) were calculated by using the TPSSh functional and the SCRECP and DKH2 approaches, with the EPR-III basis set to describe the ligand atoms. The highest spin state was considered as the ground state (octuplet, $4f^7$) in all cases. Since the calculation of HFCCs was performed by using an unrestricted model, spin contamination[56] was assessed by a comparison of the expected difference between $S(S+1)$ for the assigned spin state [$S(S+1)$=15.75 for the mononuclear Gd^{III} complexes investigated here] and the actual value of $\langle S^2\rangle$.[57] The results obtained for $[Gd(H_2O)_8]^{3+}$ indicate that spin contamination is negligible for all functionals tested in this work [$\langle S^2\rangle - S(S+1) < 0.0060$]. A similar situation holds for all Gd^{III} complexes with polyaminocarboxylate ligands investigated by using the TPSSh functional [$\langle S^2\rangle - S(S+1) < 0.0090$]. Convergence of the SCF procedure during the calculations of ^{17}O HFCCs was

problematic in some cases, and therefore a quadratically convergent SCF procedure was used when first-order SCF did not achieve convergence (by using the scf=xqc keyword in Gaussian 09). The default values for the integration grid (75 radial shells and 302 angular points) and the SCF energy convergence criteria (10^{-8}) were used in all calculations.

Throughout this work solvent effects were included by using the polarizable continuum model (PCM), in which the solute cavity is built as an envelope of spheres centered on atoms or atomic groups with appropriate radii. In particular, we used the integral equation formalism (IEFPCM) variant as implemented in Gaussian 09.[58]

Results and discussion

Calculation of ^{17}O HFCCs in $[Gd(H_2O)_8]^{3+}$

Due to its small size, DFT calculations on the $[Gd(H_2O)_8]^{3+}$ complex are relatively undemanding, and therefore we used this system to evaluate the performance of twelve commonly available density functionals (SVWN, SPL, BLYP, G96LYP, mPWLYP, BB95, TPSS, B3LYP, BH&HLYP, B3PW91, PBE1PBE and TPSSh) to predict isotropic ^{17}O HFCCs. The main results of our calculations are shown in Figure **1** and Table **1**. Experimental A_{iso} values of 0.71[59] and 0.76[50] MHz have been obtained from ^{17}O NMR shift data, while a value of 0.84[5] MHz was determined from the simultaneous analysis of ^{17}O NMR chemical shifts and ^{1}H relaxivity data.

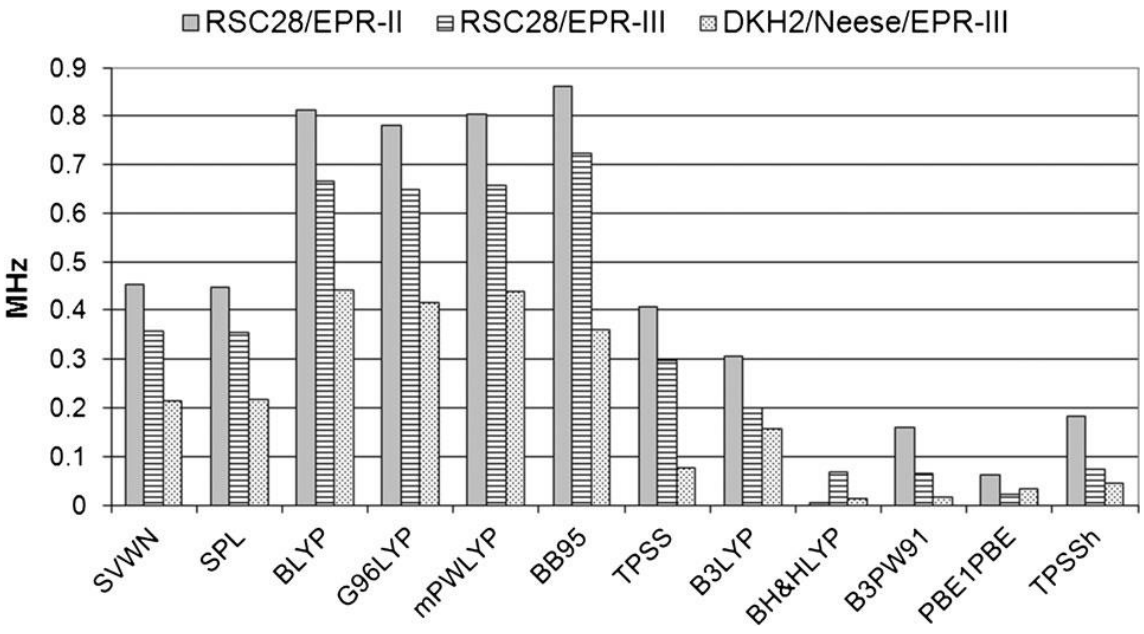

Figure 1. Absolute deviations of calculated A_{iso} values [MHz] obtained for $[Gd(H_2O)_8]^{3+}$ by using different density functionals with respect to the experimental value (0.84 MHz).

Table 1. Calculated ^{17}O hyperfine coupling constants (A_{iso}) [MHz] calculated for $[Gd(H_2O)_8]^{3+}$.

Type	Functional	Method	A_{iso}
LSDA	SVWN	RSC28/EPR-II	0.387
		RSC28/EPR-III	0.481
		DKH2/Neese/EPR-III	0.626
	SPL	RSC28/EPR-II	0.392
		RSC28/EPR-III	0.485
		DKH2/Neese/EPR-III	0.623
GGA	BLYP	RSC28/EPR-II	0.028
		RSC28/EPR-III	0.175
		DKH2/Neese/EPR-III	0.399
	G96LYP	RSC28/EPR-II	0.058
		RSC28/EPR-III	0.193
		DKH2/Neese/EPR-III	0.424
	mPWLYP	RSC28/EPR-II	0.035
		RSC28/EPR-III	0.182
		DKH2/Neese/EPR-III	0.401
Meta-GGA	BB95	RSC28/EPR-II	−0.020
		RSC28/EPR-III	0.116
		DKH2/Neese/EPR-III	0.480
	TPSS	RSC28/EPR-II	0.432
		RSC28/EPR-III	0.542
		DKH2/Neese/EPR-III	0.764
Hybrid-GGA	B3LYP	RSC28/EPR-II	0.533
		RSC28/EPR-III	0.640
		DKH2/Neese/EPR-III	0.683
	BH&HLYP	RSC28/EPR-II	0.836
		RSC28/EPR-III	0.907
		DKH2/Neese/EPR-III	0.853
	B3PW91	RSC28/EPR-II	0.679
		RSC28/EPR-III	0.776
		DKH2/Neese/EPR-III	0.824
	PBE1PBE	RSC28/EPR-II	0.777
		RSC28/EPR-III	0.861
		DKH2/Neese/EPR-III	0.873
Hybrid *meta*-GGA	TPSSh	RSC28/EPR-II	0.656
		RSC28/EPR-III	0.766
		DKH2/Neese/EPR-III	0.885

The data reported in Table **1** and Figure **1** indicate that LSDA functionals (SVWN and SPL) provide a poor agreement between the experimental and calculated A_{iso} values, with absolute deviations above 0.2 MHz. The agreement is even worse when using GGA functionals (BLYP, G96LYP or mPWLYP), which deviate by 0.42 to 0.81 MHz from the experimental value of 0.84 MHz. The performance of the meta-GGA functional BB95 is also poor, while TPSS performs somewhat better, particularly when using DKH2 calculations. These results are in agreement with previous calculations performed on small main-group

radicals and 3d and 4d transition metal complexes, which showed that meta-GGA functionals do not substantially improve the results compared to GGA functionals.[60] The use of hybrid-GGA functionals (B3LYP, BH&HLYP and B3PW91 or PBE1PBE) results in an important improvement of the agreement between the experimental and calculated A_{iso} values. This is in line with previous investigations on transition metal complexes, which established that hybrid GGA functionals provide the best predictions of HFCCs.[61,62] In the case of $[Gd(H_2O)_8]^{3+}$ the hybrid GGA functionals BH&HLYP, B3PW91 and PBE1PBE appear to perform somewhat better than B3LYP. As observed previously,[63] the hybrid variant of TPSS, TPSSh, provides a clear improvement of the calculated HFCCs in comparison to the non-hybrid counterpart. Considering the uncertainty of the experimental value of A_{iso} in $[Gd(H_2O)_8]^{3+}$, for which values ranging between 0.71 and 0.84 MHz have been reported, we conclude that hybrid GGA functionals BH&HLYP, B3PW91 and PBE1PBE, as well as the hybrid meta-GGA functional TPSSh, provide A_{iso} values in close agreement with the experimental values. The DKH2 and SCRECP approaches give A_{iso} values in good mutual agreement when using hybrid GGA and hybrid meta-GGA functionals, while the DKH2 approach provides somewhat better results with LSDA and GGA functionals. The use of the EPR-III basis set in SCRECP calculations significantly improves the agreement between experimental and calculated values with respect to RSC28/EPR-II calculations. It must be pointed out that our SCECP calculations used point charges for the nuclei, while DKH2 calculations employed a Gaussian nuclear model. Different studies showed that the use of point charges for the nuclei is not always a suitable approximation, particularly when hyperfine properties for heavy nuclei are considered.[64] Thus, the discrepancies in A_{iso} values calculated with the SCECP and DKH2 approaches, particularly when using LSDA and GGA functionals, might be related to the use of the point charge approximation for the nuclei in SCECP calculations.

Molecular geometries of Gd^{III} polyaminocarboxylates

Prior to calculation of the ^{17}O A_{iso} values of the inner-sphere water molecule in the various Gd complexes, the molecular geometries of these systems were fully optimized in aqueous solution (IEFPCM model) at the TPSSh/LCRECP/6-31G(d) level. The optimized molecular geometries of the complexes are shown in Figure **2** and the average bond distances of the metal coordination environment are given in Table **2**. The results show that our calculations reproduce the distances between Gd and the donor atoms of the ligands observed in the corresponding X-ray structures fairly well. However, the distances between Gd and the oxygen atom of the inner-sphere water molecule (2.56–2.67 Å) are clearly longer than those observed in the solid state (2.44–2.52 Å). All calculated Gd—O_W distances are also longer than that normally assumed in the analysis of ^{17}O NMR longitudinal relaxation data of nine-coordinate Gd^{III} complexes (2.50 Å),[5] and also longer than those determined experimentally by using ENDOR spectra (2.4–2.5 Å).[65] This bond elongation can be attributed, at least in part, to the fact that continuum models of solvation cannot account for specific solvent–solute interactions (i.e. hydrogen-bonding interactions between inner-sphere and second-sphere water molecules). Indeed, it has been shown that continuum dielectric solvent models are often inadequate for investigating ionic solutes that have concentrated charge densities with strong local solute–solvent interactions.[66] To overcome this deficiency of continuum solvent models, it has become a common practice to add explicit solvent molecules to the model ionic systems.[67] Thus, we performed geometry optimizations by using a mixed cluster/continuum model explicitly including second-sphere water molecules. The major disadvantage of this approach is that adding extra solvent molecules to the first solvation sphere increases the computational cost. Moreover, the more atoms are included in the system, the larger the number of degrees of freedom and the higher the number of minimum-energy structures.

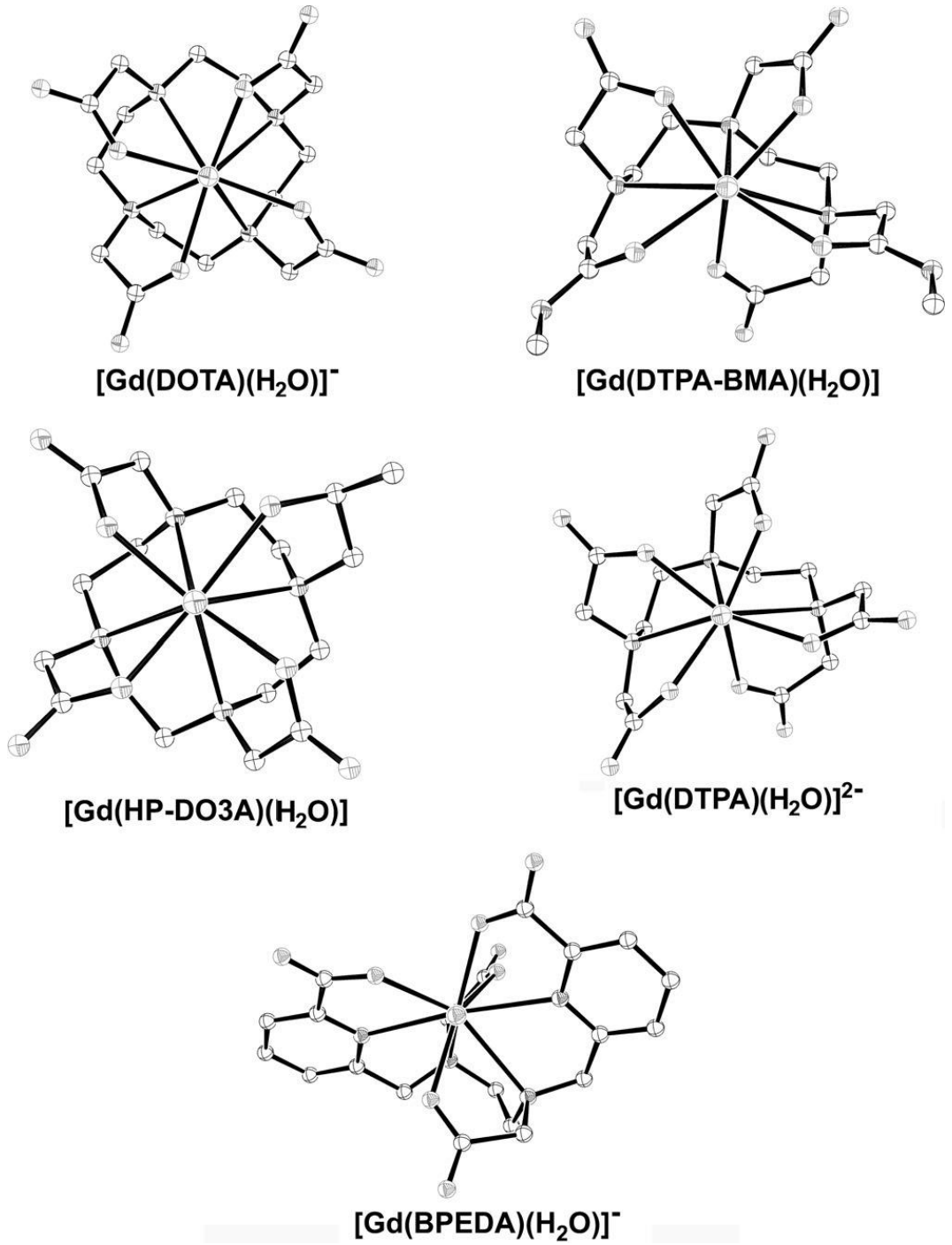

Figure 2. Structures of the $[Gd(L)(H_2O)]^{+/-}$ systems (L=BPEDA, DOTA, DTPA, DTPA-BMA or HP-DO3A) as optimized in water at the TPSSh/LCRECP/6-31G(d) level. Views are along the Gd—O_W axis.

Our calculations performed on the $[Gd(L)(H_2O)]^{+/-}\cdot x\,H_2O$ systems (L=BPEDA, DOTA, DTPA, DTPA-BMA or HP-DO3A) show that the inclusion of one second-sphere water molecule considerably shortens the Gd—O_W distances, while the inclusion of a second water molecule involved in hydrogen-bonding interaction with the inner-sphere water provides Gd—O_W distances in close agreement with the experimental values (Table **2**). Furthermore, the Gd···H_{IS} distances (H_{IS}=hydrogen atoms of the inner-sphere water molecule) calculated for the systems including two second-sphere water molecules fall within the range of 2.96–3.10 Å, the average value of the five systems investigated amounting to 3.02 Å. These values are in excellent agreement with those determined experimentally with the use of pulsed ENDOR spectroscopy (3.1±0.1

Å)[73] and neutron diffraction measurements.[2a] In each of the $[Gd(L)(H_2O)]^{+/-}\cdot 2\,H_2O$ complexes investigated the two $Gd\cdots H_{IS}$ distances are quite similar, differing by less than 0.083 Å. As an illustrative example, the optimized geometry of $[Gd(DOTA)(H_2O)]^{-}\cdot x\,H_2O$ (SAP isomer) is shown in Figure **3**. The $Gd—O_W$ distances calculated for the SAP isomer of $[Gd(DOTA)(H_2O)]^{-}\cdot x\,H_2O$ are slightly shorter than those obtained for the TSAP isomer, which is in line with a higher steric compression around the inner-sphere water molecule in the latter form.[74]

Table 2. Averaged bond distances [Å] of the metal coordination environments and ϕ angles [°] calculated at the TPSSh/LCRECP/6-31G(d) level for $[Gd(L)(H_2O)]^{n+/-}\cdot x\,H_2O$ complexes.[a]

L		*x*=0	*x*=1	*x*=2	Exp.
DOTA/SAP[b]	Gd—OC	2.383	2.394	2.394	2.365
	$Gd—N_{AM}$	2.679	2.703	2.720	2.655
	$Gd—O_W$	2.606	2.523	2.494	2.456
	ϕ	85.7	104.2	123.7	
DOTA/TSAP	$Gd—O_C$	2.394	2.396	2.398	
	$Gd—N_{AM}$	2.686	2.705	2.727	
	$Gd—O_W$	2.646	2.585	2.514	
	ϕ	83.38	92.9	121.9	
DTPA-BMA[c]	$Gd—O_C$	2.351	2.361	2.371	2.374
	$Gd—O_A$	2.551	2.520	2.521	2.441
	$Gd—N_{AM}$	2.699	2.730	2.742	2.672
	$Gd—O_W$	2.559	2.494	2.483	2.442
	ϕ	103.8	125.1	118.0	
HP-DO3A[d]	$Gd—O_C$	2.366	2.366	2.372	2.375
	$Gd—O_H$	2.495	2.495	2.533	2.330
	$Gd—N_{AM}$	2.666	2.661	2.677	2.647
	$Gd—O_W$	2.568	2.544	2.514	2.507
	ϕ	88.7	101.9	120.2	
DTPA[e]	$Gd—O_C$	2.407	2.416	2.412	2.400
	$Gd—N_{AM}$	2.673	2.711	2.743	2.640
	$Gd—O_W$	2.639	2.542	2.501	2.490
	ϕ	83.6	102.0	127.7	
BPEDA[f]	$Gd—O_C$	2.391	2.380	2.394	2.46
	$Gd—O_{PY}$	2.417	2.419	2.433	2.43
	$Gd—N_{AM}$	2.768	2.787	2.792	2.69
	$Gd—N_{PY}$	2.659	2.682	2.698	2.61
	$Gd—O_W$	2.669	2.551	2.516	2.52
	ϕ	86.4	113.4	121.7	

[a] O_C: coordinated oxygen atoms of acetate groups; O_{PY}: coordinated oxygen atoms of pyridylcarboxylate groups; N_{AM}: amine nitrogen atoms; N_{PY}: pyridyl nitrogen atoms; O_A: oxygen atoms of amide groups; O_H: oxygen atoms of hydroxyl groups; O_W: oxygen atom of inner-sphere water molecules. [b] Experimental data from ref. [68]. [c] Experimental data for the [Gd(DTPA-BBA)] complex, which crystallizes in *cis* conformation, from ref. [69]. [d] Experimental data from ref. [70]. [e] Experimental data from ref. [71]. [f] Experimental data from ref. [72].

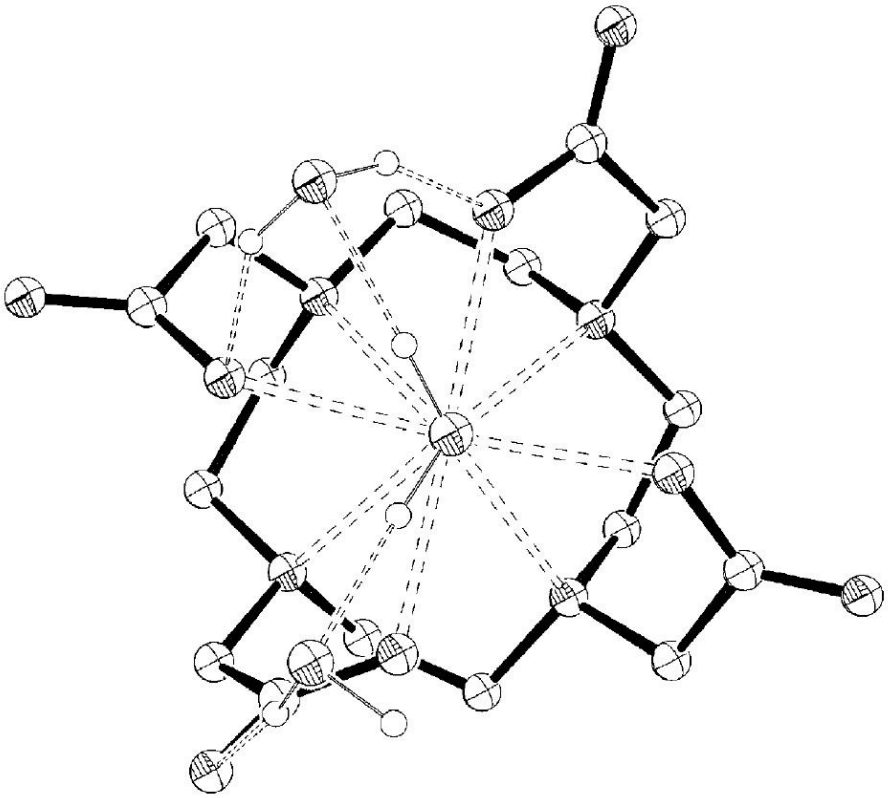

Figure 3. View along the Gd—O_W axis of the structure of $[Gd(DOTA)(H_2O)]^{-}\cdot 2\,H_2O$ (SAP isomer) as optimized in water at the TPSSh/LCRECP/6-31G(d) level showing hydrogen-bonding interactions involving inner- and second-sphere water molecules. Hydrogen atoms, except those of water molecules, are omitted for simplicity.

These results show that the explicit inclusion of a few second-sphere water molecules is crucial for the computation of accurate Gd—O_W distances in complexes with polyaminocarboxylate ligands. Additionally, the inclusion of second-sphere water molecules also affects the orientation of the inner sphere water molecule with respect to the Gd—O axis, as given by the tilt angle ϕ defined in Figure **4**. Indeed, the inner-sphere water molecule in $[Gd(L)(H_2O)]^{n+/-}$ complexes is tilted due to the hydrogen-bonding interaction established between hydrogen atoms of the water molecule and the negatively charged oxygen atoms of the ligand, which results in ϕ angles of about 85°. In the $[Gd(L)(H_2O)]^{+/-}\cdot 2\,H_2O$ systems the inner-sphere water molecule is involved in hydrogen-bonding interaction with second sphere water molecules rather than with oxygen atoms of the ligand, thereby increasing ϕ to about 120° (Table **2**).

As a general trend, the inclusion of second-sphere water molecules provokes a slight lengthening of the Gd—ligand bonds. The distances calculated for the $[Gd(L)(H_2O)]^{+/-}\cdot 2\,H_2O$ systems generally differ ≤4 % from the crystallographic reference data of the hydrated complexes. The calculated Gd—O_C distances [O_C=oxygen atoms of carboxylate groups] present an excellent agreement with the experimental values observed in the solid state. The distances between Gd and the N donor atoms of the ligands are overestimated by our calculations by 0.04–0.10 Å with respect to the X-ray values, as previously observed for related systems.[32,75]

The distances between the Gd^{III} ion and the H atoms of second-sphere water molecules in $[Gd(L)(H_2O)]^{+/-}\cdot 2H_2O$ fall within the range 3.32–5.10 Å (Table S1, Supporting Information), with an average value of 4.18 Å. The average distance between Gd and the oxygen atoms of second-sphere water molecules is slightly longer (4.25 Å), as second-sphere water molecules tend to orientate their H atoms to negatively charged groups of the ligand. These values could be taken as a reference for the analysis of

longitudinal ^{1}H and ^{17}O relaxation data of Gd-based MRI contrast agents containing a high negative charge. For such systems, it has been shown that second-sphere water molecules provide a substantial contribution to ^{1}H relaxivity and longitudinal ^{17}O relaxation rates, both related to $1/r^6$.[76]

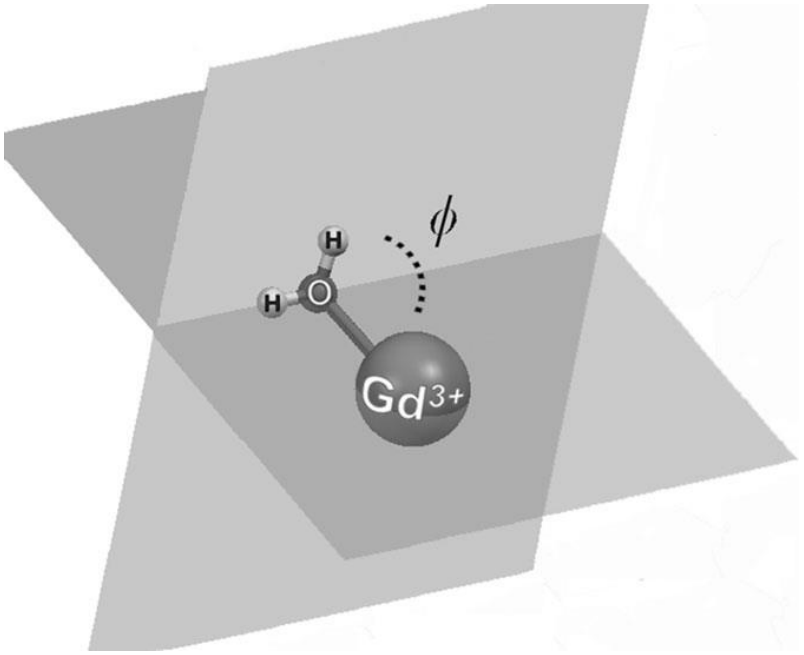

Figure 4. Definition of the tilt angle ϕ formed between the inner-sphere water molecule and the Gd—O axis.

Calculation of ^{17}O HFCCs of the coordinated water molecule in $[Gd(DTPA)(H_2O)]^{2-}\cdot x\,H_2O$

The ^{17}O A_{iso} values of the inner-sphere water molecule in the $[Gd(DTPA)(H_2O)]^{2-}\cdot x\,H_2O$ systems were calculated with the aid of the TPSSh functional in combination with the DKH2 and SCRECP approaches. The TPSSh functional was selected for this purpose on the basis of the results for $[Gd(H_2O)_8]^{3+}$ presented above. Calculations performed on the $[Gd(DTPA)(H_2O)]^{2-}$ complex provided ^{17}O A_{iso} values of ca. 0.10 and 0.08 MHz by using the ECP and DKH2 approaches, respectively. These values deviate by ca. 0.5 MHz from the experimental values of 0.61 and 0.54 MHz obtained from the analysis of the ^{17}O NMR data (Table **3**). Inclusion of one second-sphere water molecule pushes the calculated values (~0.3 MHz) closer to the experimental one, while the inclusion of two second-sphere water molecules provides calculated A_{iso} values in reasonable agreement with the experiment (0.50 and 0.52 MHz for the DKH2 and ECP approaches, respectively). Thus, the explicit consideration of the most important hydrogen-bonding interactions involving the coordinated water molecule and the second coordination shell appears to be crucial for an accurate calculation of ^{17}O A_{iso} values of the inner-sphere water molecule.

As pointed out previously,[17a] an important parameter influencing the ^{17}O HFCCs is the Gd—O distance. Thus, we performed a relaxed potential energy surface scan on the $[Gd(DTPA)(H_2O)]^{2-}$ system where the Gd—O distance was varied from 2.41 to 2.79 Å in steps of 0.015 Å. Subsequently, A_{iso} was calculated for each of these points at the RSC28/EPR-III level (Figure **5**). The variation of the Gd—O distance also provoked a substantial change of the tilt angle ϕ, which increased from 76.9° to 93.5° as the Gd—O distance was reduced from 2.79 to 2.41 Å. Our results show that A_{iso} increases from 0.028 to 0.33 MHz as the Gd—O distance decreases from 2.79 to 2.41 Å. These results highlight the importance of an accurate calculation of the Gd—O distance to obtain A_{iso} values in close agreement with the experimental data. However, these

calculations provide a A_{iso} value of 0.23 MHz for Gd—O distance of 2.49 Å, which corresponds to the distance observed in the solid state for the $[Gd(DTPA)(H_2O)]^{2-}$ complex. Considering the experimental values of A_{iso} reported in the literature, 0.61 and 0.54 MHz,[5,77] we conclude that the Gd—O distance is not the only factor affecting the magnitude of the ^{17}O HFCC of inner-sphere water molecules of Gd^{III} complexes. Indeed, further calculations performed on the $[Gd(DTPA)(H_2O)]^{2-}$ complex show that the orientation of the water molecule with respect to the Gd—O axis has a strong influence on the calculated HFCCs too (Figure **6**). For a fixed Gd—O distance of 2.504 Å the calculated A_{iso} values increase from 0.22 to 0.58 MHz as the ϕ angle increases from 89.6 to 180°. A ϕ value of about 90° implies that the water molecule uses a lone-pair placed on a p orbital to bind Gd. As the tilt angle increases, the s character of the lone pair is increasing, which increases the probability of the unpaired spin density to sit just on the nucleus, resulting in an increased A_{iso}.

Table 3. Calculated hyperfine coupling constants (A_{iso}) [MHz] for $[GdL(H_2O)]^{n+/-}\cdot xH_2O$ complexes (TPSSh model).

L		x=0	x=1	x=2	Exp.
DTPA	RSC28/EPR-III	0.097	0.290	0.518	0.605[a]
	DKH2/Neese/EPR-III	0.077	0.271	0.499	0.541[b]
DOTA/SAP	RSC28/EPR-III	0.140	0.371	0.561	0.590[c]
	DKH2/Neese/EPR-III	0.123	0.357	0.547	
DOTA/TSAP	RSC28/EPR-III	0.083	0.266	0.509	
	DKH2/Neese/EPR-III	0.064	0.245	0.490	
DTPA-BMA	RSC28/EPR-III	0.304	0.537	0.557	0.605[a]
	DKH2/Neese/EPR-III	0.286	0.518	0.543	
HP-DO3A	RSC28/EPR-III	0.179	0.279	0.434	0.462[d]
	DKH2/Neese/EPR-III	0.161	0.261	0.416	
BPEDA	RSC28/EPR-III	0.007	0.238	[f]	0.368[e]
	DKH2/Neese/EPR-III	−0.014	0.220	0.396	

[a] Ref. [5]. [b] Ref. [77]. [c] Ref. [5]. The Gd DOTA complex is known to exist in solution as a mixture of SAP and TSAP isomers, with the SAP form representing ca. 85 % of the overall population (see text). [d] Ref. [11]. [e] Ref. [10]. [f] SCF convergence problems prevented the calculation of A_{iso}.

The spin density distribution in a given paramagnetic molecule denotes the difference between the contributions due to electrons with majority spin (α) and minority spin (β), and is the result of two effects: 1) spin delocalization, that is, the transmission of spin density through the bonds towards the observed nucleus; 2) spin polarization, which is the result of an effective attraction of unpaired electrons to the nearby ones of the same spin. Spin delocalization gives always a positive contribution to the spin density in contrast to spin polarization which can lead to a positive or negative contribution.[18] Figure **7** shows a spin density map calculated for $[Gd(DTPA)(H_2O)]^{2-}\cdot 2\,H_2O$ at the RSC28/EPR-III level. As found previously for $[Gd(H_2O)_8]^{3+}$,[17a,18] the negative spin density calculated at the coordinated water oxygen indicates domination of the spin-polarization effect at this location. Most of the positive spin density is placed on the Gd^{III} ion itself. This shows that spin-polarization effects dominate the ^{17}O A_{iso} values of the coordinated water molecule in Gd^{III} complexes. It is worth to recall that the negative spin density at the ^{17}O nucleus of the inner-sphere water molecule corresponds to a positive A_{iso} value (+0.518 MHz, Table **3**) as a consequence of the negative magnetic moment of the ^{17}O nucleus.

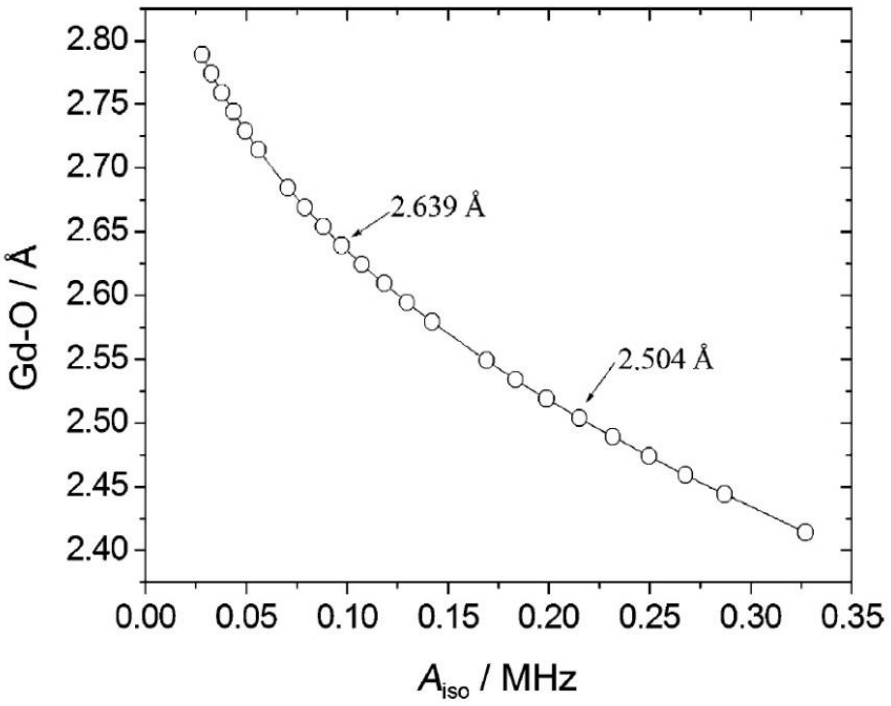

Figure 5. Dependence of the ^{17}O A_{iso} values with the Gd—O distance in $[Gd(DTPA)(H_2O)]^{2-}$ as calculated at the RSC28/EPR-III level. The arrows indicate the data obtained for the equilibrium geometry of $[Gd(DTPA)(H_2O)]^{2-}$ (Gd—O_W=2.639 Å, A_{iso}=0.097 MHz), and the Gd—O_W distance used to scan ϕ in Figure 6. This distance is close to that found for $[Gd(DTPA)(H_2O)]^{2-}\cdot 2\ H_2O$ (2.501 Å).

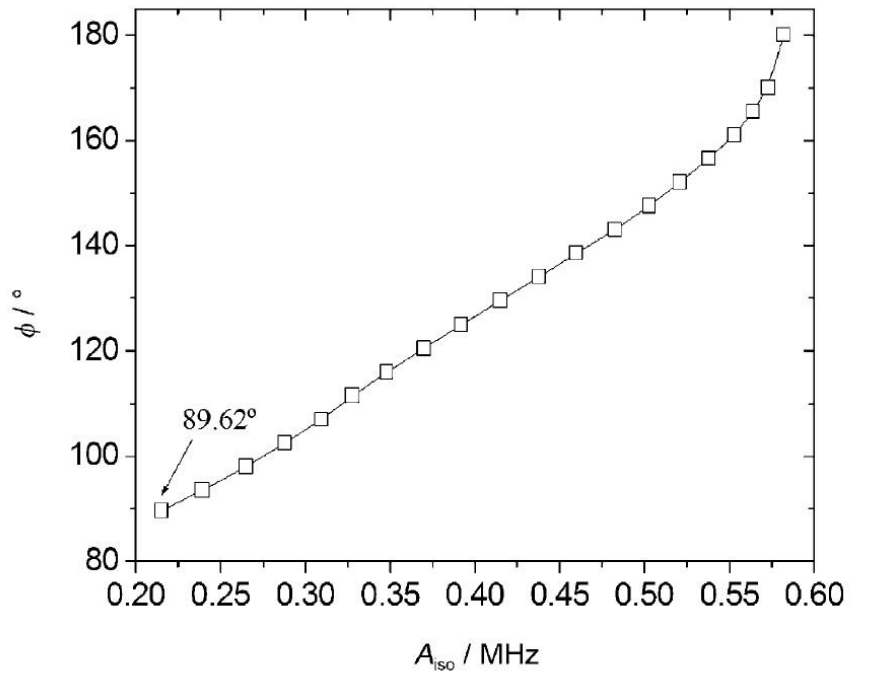

Figure 6. Dependence of the A_{iso} values with tilt angle ϕ at a fixed Gd—O distance of 2.504 Å in $[Gd(DTPA)(H_2O)]^{2-}$ (RSC28/EPR-III level). The arrow indicates the torsion angle obtained from geometry optimization when the Gd—O distance is fixed at 2.504 Å.

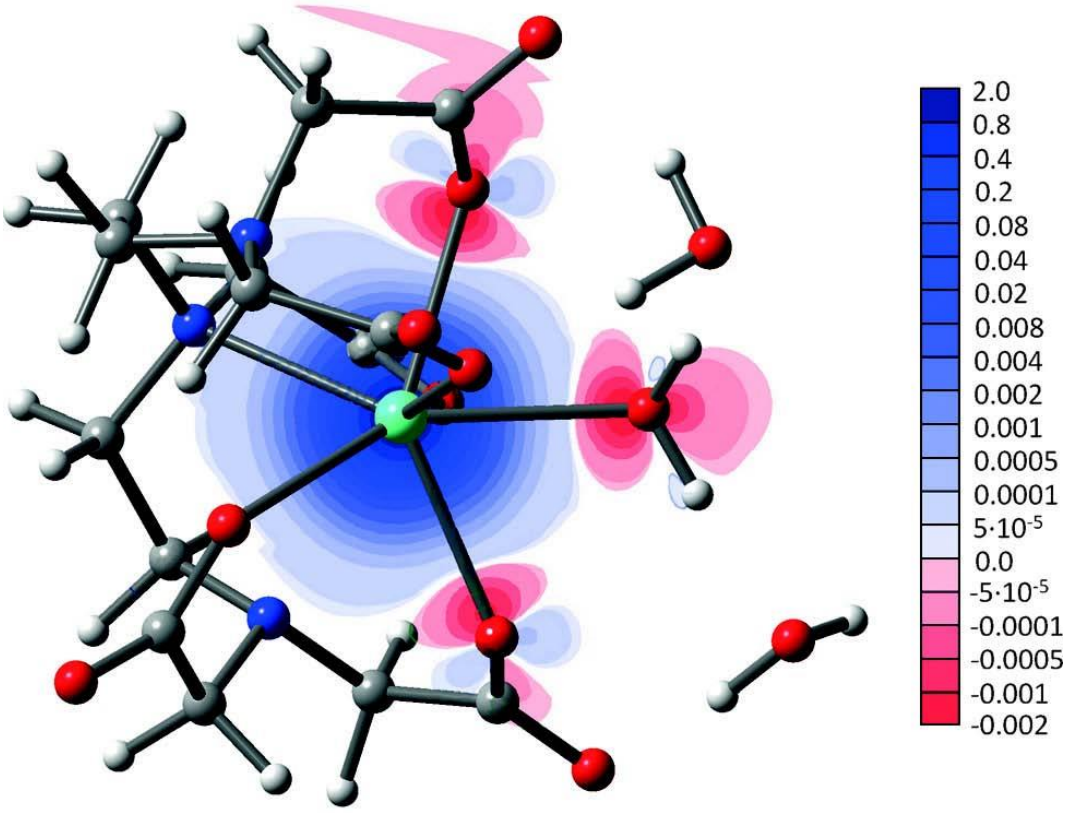

Figure 7. Contour spin density map obtained for the $[Gd(DTPA)(H_2O)]^{2-}\cdot 2\,H_2O$ system at the RSC28/EPR-III level on the plane defined by the Gd atom, the oxygen atom of the coordinated water molecule and one of its hydrogen atoms [in au^{-3}].

Calculation of ^{17}O HFCCs in related systems

Calculations performed on $[Gd(L)(H_2O)]^{n+/-}$ complexes without second-sphere water molecules confirm the poor agreement of calculated A_{iso} with experimental data. Inclusion of only two second-sphere water molecules hydrogen-bonded to the first-sphere H_2O molecule results in calculated HFCCs in close agreement with the experimental data. Furthermore, RSC28/EPR-III and DKH2/Neese/EPR-III calculations provide similar results, with the latter giving A_{iso} values typically 0.02 MHz smaller than the former (Table **3**). The results suggest that the small experimental HFCCs determined for $[Gd(BPEDA)(H_2O)]^-$ and [Gd(HP-DO3A)(H_2O)] were correctly determined, and that in some cases the HFCCs might fall out of the generally accepted $3.9\pm0.3\times10^6$ rad s^{-1} (A_{iso}=0.67–0.57 MHz) range. A close inspection of the data reported in Tables **2** and **3** shows that the calculated A_{iso} values roughly correlate with the calculated Gd—O_W distances (Figure **8**). From Figure **8** it can be seen that A_{iso} calculated for $[Gd(DTPA\text{-}BMA)(H_2O)]\cdot 2\,H_2O$ is low, considering its particularly short Gd—O_W distance. The offset from the linear correlation can be partially ascribed to the small Gd—O—H—H torsion angle (118.0°) calculated from the optimized structure. The A_{iso} values obtained for the TSAP isomer of $[Gd(DOTA)(H_2O)]^-\cdot 2\,H_2O$ are ~10 % lower than those determined for the SAP isomer, in agreement with the shorter Gd—O_W distance for the latter. The population of the TSAP isomer of $[Gd(DOTA)(H_2O)]^-$ in solution is relatively small (ca. 15 %),[33] and therefore the ^{17}O HFCC determined experimentally is expected to be dominated by that of the SAP isomer.

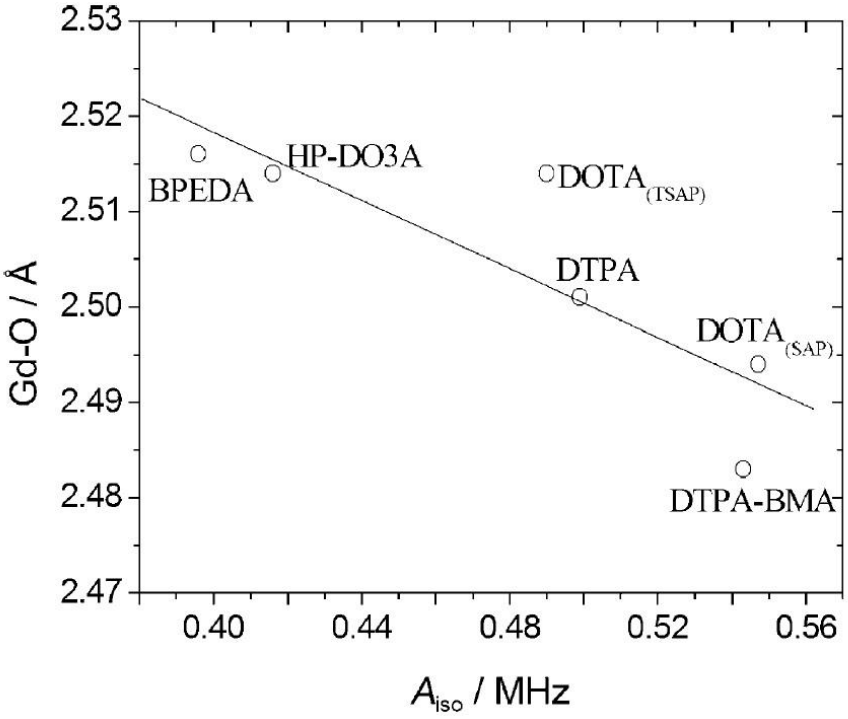

Figure 8. Correlation between Gd—O distances and A_{iso} values calculated for $[Gd(L)(H_2O)]^{n+/-}$ $2H_2O$ complexes at the DKH2/Neese/EPR-III level.

An advantage using snapshots from MD simulations for the calculation of HFCCs is the inclusion of solution dynamics on the calculated A_{iso} values.[18] However, the data shown in Figures **5** and **6** indicate an approximately linear dependence of A_{iso} around the equilibrium configuration with respect to both the Gd—O_W distance and the ϕ angle. The measured HFCCs are weighted averages ($<A_{iso}>$) of individual values for different configurations present in solution. It is therefore not expected that $<A_{iso}>$ differs substantially from the value corresponding to the equilibrium geometry. The good agreement between the experimental and calculated HFCCs given in Table **3** are in line with this reasoning. Furthermore, previous molecular dynamics studies performed on the $[Gd(DOTA)(H_2O)]^-$ system pointed to a relatively narrow distribution width of A_{iso} (0.58±0.11 MHz).[18]

The calculations performed on the $[Gd(L)(H_2O)]^{n+/-}\cdot x\,H_2O$ systems allow to evaluate ^{17}O HFCCs of second-sphere water molecules, which could provide a non-negligible scalar contribution to the observed ^{17}O NMR chemical shifts. Indeed, different experimental works assumed that the outer-sphere contribution can be accounted for by an empirical constant C_{OS} [Eq. (5)], with fitted values of 0.0–0.2. Thus, according to these studies, the outer-sphere contribution to the observed chemical shifts may be responsible of up to 20 % of the observed chemical shifts. The A_{iso} values obtained for second-sphere water molecules (A_{iso}^{ss}, Table **4**) are close to zero, and their absolute values amount to 1.5–3.6 % of those calculated for the coordinated water molecule. Again, both the RSC28/EPR-III and DKH2/Neese/EPR-III approaches provide results in good mutual agreement. Furthermore, our calculations provide negative A_{iso}^{ss} values, which suggest that the scalar contribution of second-sphere water molecules to the overall observed ^{17}O chemical shifts might be negligible, or result in slightly reduced observed chemical shifts.

Table 4. Calculated ^{1}H HFCCs of inner-sphere water molecules (A_{iso}, MHz) and ^{17}O HFCCs of second-sphere water molecules (A_{iso}^{ss}) [MHz] in $[GdL(H_2O)]^{n+/-}\cdot 2\ H_2O$ complexes (TPSSh model).

Type	Method	A_{iso}^{ss}, ^{17}O	A_{iso}, ^{1}H
DTPA	RSC28/EPR-III	-8.4×10^{-3}	0.056
		-6.0×10^{-3}	0.039
	DKH2/Neese/EPR-III	−0.010	0.070
		-7.9×10^{-3}	0.055
DOTA/SAP	RSC28/EPR-III	−0.013	0.051
		-2.3×10^{-3}	0.085
	DKH2/Neese/EPR-III	−0.015	0.067
		-4.0×10^{-3}	0.099
DOTA/TSAP	RSC28/EPR-III	-4.7×10^{-3}	0.054
		-7.4×10^{-3}	0.056
	DKH2/Neese/EPR-III	-6.3×10^{-3}	0.070
		-8.7×10^{-3}	0.070
DTPA-BMA	RSC28/EPR-III	-7.8×10^{-3}	0.054
		−0.013	0.076
	DKH2/Neese/EPR-III	-9.0×10^{-3}	0.073
		−0.015	0.092
HP-DO3 A	RSC28/EPR-III	−0.013	0.073
		−0.013	0.099
	DKH2/Neese/EPR-III	−0.014	0.085
		−0.015	0.108
BPEDA	RSC28/EPR-III	[a]	[a]
	DKH2/Neese/EPR-III	-9.5×10^{-3}	0.058
		2.7×10^{-3}	0.068

[a] SCF convergence problems prevented the calculation of A_{iso}.

<u>^{1}H HFCCs of the coordinated water molecules</u>

As expected, the calculated ^{1}H isotropic HFCCs for the systems investigated herein are quite small. For $[Gd(H_2O)_8]^{3+}$ our calculations provide ^{1}H A_{iso} values of −0.031 (RSC28/EPR-III) and −0.012 (DKH2/Neese/EPR-III), which compare well with the experimental values (−0.015 to 0.04 MHz) obtained from EPR studies.[78] Previous DFT calculations performed by Helm and coworkers provided a small ^{1}H A_{iso}, which was however found to be positive (+0.025).[17a] A positive value was also found for $[Gd(H_2O)_8]^{3+}$ from ENDOR experiments (0.03±0.02 MHz).[73] The ^{1}H A_{iso} values calculated for the $[Gd(L)(H_2O)]^{n+/-}\cdot 2\ H_2O$ complexes were found to be positive (Table **4**), in agreement with the value obtained for the complex of HP-DO3 A from ENDOR experiments (+0.04±0.06*)* MHz.[73] The small absolute values and different signs obtained both experimentally and computationally for ^{1}H HFCCs in different Gd^{III} complexes are attributed to the fact that the hydrogen atoms lie close to the node of the spin density, as illustrated in Figure **7** for $[Gd(DTPA)(H_2O)]^{2-}\cdot 2\ H_2O$. All experimental and calculated ^{1}H A_{iso} values of coordinated water molecules are close to zero, which confirms that the scalar contribution to ^{1}H relaxivity can be safely neglected.

Conclusions

We have evaluated the performance of twelve commonly available functionals for the calculations of ^{17}O HFCCs in $[Gd(H_2O)_8]^{3+}$. Our results show that both hybrid GGA functionals (BH&HLYP, B3PW91 and PBE1PBE) and the hybrid meta-GGA functional TPSSh provide A_{iso} values in close agreement with the experimental data, while functionals based on the LSDA, GGA and meta-GGA approximations perform poorly. Calculations performed on $[Gd(L)(H_2O)]^{n+/-}$ complexes (L=BPEDA, DOTA, DTPA, DTPA-BMA or HP-DO3A) gave ^{17}O A_{iso} values deviating up to 100 % from the experimental data obtained from ^{17}O NMR shifts and relaxation data. However, the use of a mixed cluster/continuum approach with the explicit inclusion of two second-sphere water molecules during geometry optimization allowed us to calculate accurate HFCCs for these complexes. The DKH2/Neese/EPR-III and RSC28/EPR-III approaches were shown to provide calculated HFCCs of essentially the same quality.

The theoretical investigation reported here shows that the ^{17}O HFCCs on inner-sphere water molecules are sensitive not only to the Gd—O distances, but also to the orientation of the coordinated water molecule plane and the Gd—O vector. Small changes of these structural parameters result in relatively important changes on the isotropic ^{17}O HFCCs, which in some particular cases might deviate from the generally accepted range of 0.67–0.57 MHz. Additionally, our calculations suggest that the outer-sphere contribution to the observed ^{17}O NMR chemical shifts can safely be neglected, as well as the scalar contribution to ^{1}H relaxivity, which is clearly dominated by the dipolar mechanism. We believe that the independent calculation of isotropic ^{17}O HFCCs following the methodology presented herein will allow a more reliable fitting of experimental ^{17}O NMR data, thereby providing more accurate values of the parameters governing the relaxivity in Gd complexes with potential application in MRI.

Acknowledgements

The authors thank Ministerio de Educación y Ciencia (MEC, CTQ2009-10721), Fondo Europeo de Desarrollo Regional (FEDER, CTQ2009-10721) and Xunta de Galicia (IN845B-2010/063) for financial support. The authors are also indebted to Centro de Supercomputación de Galicia (CESGA) for providing the computer facilities.

Supporting information

Supporting information for this article is available online: https://doi.org/10.1002/cphc.201200417.

References

[1] *The Chemistry of Contrast Agents in Medical Magnetic Resonance Imaging* (Eds: A. E. Merbach, É. Tóth), Wiley, New York, **2001**.

[2] a) P. Caravan, J. J. Ellinson, T. J. McMurry, R. B. Lauffer, *Chem. Rev*. **1999**, *99*, 2293–2352; b) L. M. De Leon-Rodriguez, A. J. M. Lubag, C. Malloy, G. V. Martinez, R. J. Gillies, A. D. Sherry, *Acc. Chem. Res.* **2009**, *42*, 948–957; c) K. W.-Y. Chan, W.-T. Wong, *Coord. Chem. Rev*. **2007**, *251*, 2428–2451; d) E. Terreno, D. D. Castelli, A. Viale, S. Aime, *Chem. Rev*. **2010**, *110*, 3019–3042.

[3] a) I. Solomon, *Phys. Rev*. **1955**, *99*, 559–565; b) I. Solomon, N. Bloembergen, *J. Chem. Phys*. **1956**, *25*, 261–266; c) N. Bloembergen, *J. Chem. Phys*. **1957**, *27*, 572–573; d) N. Bloembergen, L. O. Morgan, *J. Chem. Phys*. **1961**, *34*, 842–850.

[4] J. H. Freed, *J. Chem. Phys*. **1978**, *68*, 4034–4037.

[5] D. H. Powell, O. M. Ni Dhubhghaill, D. Pubanz, L. Helm, Y. S. Lebedev, W. Schlaepfer, A. E. Merbach, *J. Am. Chem. Soc*. **1996**, *118*, 9333–9346.

[6] a) F. A. Dunand, A. Borel, A. E. Merbach, *J. Am. Chem. Soc*. **2002**, *124*, 710–716; b) F. Yerly, K. I. Hardcastle, L. Helm, S. Aime, M. Botta, A. E. Merbach, *Chem. Eur. J*. **2002**, *8*, 1031–1039.

[7] a) G. Dehaen, P. Verwilst, S. V. Eliseeva, S. Laurent, L. Vander Elst, R. N. Muller, W. M. De Borggraeve, K. Binnemans, T. N. Parac-Vogt, *Inorg. Chem*. **2011**, *50*, 10005–10014; b) M. Botta, S. Avedano, G. B. Giovenzana, A. Lombardi, D. Longo, C. Cassino, L. Tei, S. Aime, *Eur. J. Inorg. Chem*. **2011**, 802–810; c) Y.-H. Chang, C.-Y. Chen, G. Singh, H.-Y. Chen, G.-C. Liu, Y.-G. Goan, S. Aime, Y.-M. Wang, *Inorg. Chem*. **2011**, *50*, 1275–1287; d) V. Kubíček, A. Hamplová, L. Maribé, S. Mameri, R. Ziessel, E. Tóth, L. Charbonnière, *Dalton Trans*. **2009**, 9466–9474; e) P. Caravan, G. Parigi, J. M. Chasse, N. J. Cloutier, J. J. Ellison, R. B. Lauffer, C. Luchinat, S. A. McDermid, M. Spiller, T. J. McMurry, *Inorg. Chem*. **2007**, *46*, 6632–6639; f) J. Rudovský, M. Botta, P. Hermann, A. Koridze, S. Aime, *Dalton Trans*. **2006**, 2323–2333.

[8] M. C. Alpoim, A. M. Urbano, C. F. G. C. Geraldes, J. A. Peters, *J. Chem. Soc. Dalton Trans*. **1992**, 463–467.

[9] A. Rodríguez-Rodríguez, D. Esteban-Gómez, A. de Blas, T. Rodríguez-Blas, M. Fekete, M. Botta, R. Tripier, C. Platas-Iglesias, *Inorg. Chem*. **2012**, *51*, 2509–2521.

[10] C. Platas-Iglesias, M. Mato-Iglesias, K. Djanashvili, R. N. Muller, L. Vander Elst, J. A. Peters, A. de Blas, T. Rodríguez-Blas, *Chem. Eur. J*. **2004**, *10*, 3579–3590.

[11] S. Laurent, L. Vander Elst, R. N. Muller, *Contrast Media Mol. Imaging* **2006**, *1*, 128–137.

[12] a) N. Graeppi, D. H. Powell, G. Laurenczy, L. Zekany, A. E. Merbach, *Inorg. Chim. Acta* **1995**, *235*, 311–326; b) E. Tóth, O. M. Ni Dhubhghaill, G. Besson, L. Helm, A. E. Merbach, *Magn. Reson. Chem*. **1999**, *37*, 701–708.

[13] a) C. Platas-Iglesias, D. M. Corsi, L. Vander Elst, R. N. Muller, D. Imbert, J.-C. G. Bünzli, E. Tóth, T. Maschmeyer, J. A. Peters, *Dalton Trans.* **2003**, 727–737; b) M. Mato-Iglesias, A. Roca-Sabio, Z. Palinkas, D. Esteban-Gómez, C. Platas-Iglesias, E. Tóth, A. de Blas, T. Rodríguez-Blas, *Inorg. Chem*. **2008**, *47*, 7840–7851; c) E. Balogh, M. Mato-Iglesias, C. Platas-Iglesias, E. Tóth, K. Djanashvili, J. A. Peters, A. de Blas, T. Rodríguez-Blas, *Inorg. Chem*. **2006**, *45*, 8719–8728.

[14] A. R. Al Derzi, S. Fau, R. J. Bartlett, *J. Phys. Chem. A* **2003**, *107*, 6656–6667.

[15] V. Barone, P. Cimino, A. Pedone, *Magn. Reson. Chem*. **2010**, *48*, S11–S22.

[16] a) A. C. Saladino, S. C. Larsen, *Catal. Today* **2005**, *105*, 122–133; b) J. Schraut, A. V. Arbuznikov, S. Schinzel, M. Kaupp, *ChemPhysChem* **2011**, *12*, 3170–3179.

[17] a) O. V. Yazyev, L. Helm, V. G. Malkin, O. L. Malkina, *J. Phys. Chem. A* **2005**, *109*, 10997–11005; b) O. V. Yazyev, L. Helm, *J. Chem. Phys*. **2007**, *127*, 084506.

[18] O. V. Yazyev, L. Helm, *Eur. J. Inorg. Chem*. **2008**, 201–211.

[19] F. Neese, *Coord. Chem. Rev*. **2009**, *253*, 526–563.

[20] a) J. R. Zimmerman, W. E. Brittin, *J. Phys. Chem*. **1957**, *61*, 1328–1333; b) T. J. Swift, R. E. Connick, *J. Chem. Phys*. **1962**, *37*, 307–320; c) J. S. Leigh, Jr., *J. Magn. Reson*. **1971**, *4*, 308–311; A. C. McLaughlin, J. S. Leigh, Jr., *J. Magn. Reson*. **1973**, *9*, 296–304.

[21] A. D. McLachlan, *Proc. R. Soc. London Ser. A* **1964**, *280*, 271–288.

[22] B. Bleaney, *J. Magn. Reson*. **1972**, *8*, 91–100.

[23] R. V. Southwood-Jones, W. L. Earl, K. E. Newman, A. E. Merbach, *J. Chem. Phys*. **1980**, *73*, 5909–5918.

[24] Gaussian 09 (Revision B.1), M. J. Frisch, G. W. Trucks, H. B. Schlegel, G. E. Scuseria, M. A. Robb, J. R. Cheeseman, G. Scalmani, V. Barone, B. Mennucci, G. A. Petersson, H. Nakatsuji, M. Caricato, X. Li, H. P. Hratchian, A. F. Izmaylov, J. Bloino, G. Zheng, J. L. Sonnenberg, M. Hada, M. Ehara, K. Toyota, R. Fukuda, J. Hasegawa, M. Ishida, T. Nakajima, Y. Honda, O. Kitao, H. Nakai, T. Vreven, J. A. Montgomery, Jr., J. E. Peralta, F. Ogliaro, M. Bearpark, J. J. Heyd, E. Brothers, K. N. Kudin, V. N. Staroverov, R. Kobayashi, J. Normand, K. Raghavachari, A. Rendell, J. C. Burant, S. S. Iyengar, J. Tomasi, M. Cossi, N. Rega, J. M. Millam, M. Klene, J. E. Knox, J. B. Cross, V. Bakken, C. Adamo, J. Jaramillo, R. Gomperts, R. E. Stratmann, O. Yazyev, A. J. Austin, R. Cammi, C. Pomelli, J. W. Ochterski, R. L. Martin, K. Morokuma, V. G. Zakrzewski, G. A. Voth, P. Salvador, J. J. Dannenberg, S. Dapprich, A. D. Daniels, Ö. Farkas, J. B. Foresman, J. V. Ortiz, J. Cioslowski, D. J. Fox, Gaussian, Inc., Wallingford, CT, **2009**.

[25] P. Pyykkö, *Chem. Rev*. **1988**, *88*, 563–594.

[26] C. van Wüllen, *J. Comput. Chem*. **1999**, *20*, 51–62.

[27] a) H. Stoll, B. Metz, M. Dolg, *J. Comput. Chem*. **2002**, *23*, 767–778; b) P. Schwerdtfeger, *ChemPhysChem* **2011**, *12*, 3143–3155.

[28] M. Dolg, H. Stoll, A. Savin, H. Preuss, *Theor. Chim. Acta* **1989**, *75*, 173–194.

[29] M. Dolg, H. Stoll, H. Preuss, *J. Chem. Phys*. **1989**, *90*, 1730–1734.

[30] Energy-consistent ECPs and associated basis sets are available at http://www.theochem.uni-stuttgart.de/index.en.html.

[31] J. M. Tao, J. P. Perdew, V. N. Staroverov, G. E. Scuseria, *Phys. Rev. Lett*. **2003**, *91*, 146401.

[32] F. Mayer, C. Platas-Iglesias, L. Helm, J. A. Peters, K. Djanashvili, *Inorg. Chem*. **2012**, *51*, 170–178.

[33] S. Aime, M. Botta, M. Fasano, M. P. M. Marques, C. F. G. C. Geraldes, D. Pubanz, A. E. Merbach, *Inorg. Chem*. **1997**, *36*, 2059–2068.

[34] Z. Tyeklár, S. U. Dunham, K. Midelfort, D. M. Scott, H. Sajiki, K. Ong, R. B. Lauffer, P. Caravan, T. J. McMurry, *Inorg. Chem*. **2007**, *46*, 6621–6631.

[35] a) H. Lammers, F. Maton, D. Pubanz, M. W. van Laren, H. van Bekkum, A. E. Merbach, R. N. Muller, J. A. Peters, *Inorg. Chem*. **1997**, *36*, 2527–2538; b) U. Cosentino, D. Pitea, G. Moro, V. Barone, A. Villa, R. N. Muller, F. Botteman, *Theor. Chem. Acc*. **2004**, *111*, 204–209.

[36] a) C. Platas-Iglesias, A. Roca-Sabio, M. Regueiro-Figueroa, D. Esteban-Gómez, A. De Blas, T. Rodríguez-Blas, *Curr. Inorg. Chem*. **2011**, *1*, 91–116; b) C. Platas-Iglesias, *Eur. J. Inorg. Chem*. **2012**, 2023–2033.

[37] J. C. Slater, *The Self-Consistent Field for Molecular and Solids, Quantum Theory of Molecular and Solids, Vol. 4*, McGraw-Hill, New York, **1974**.

[38] S. H. Vosko, L. Wilk, M. Nusair, *Can. J. Phys*. **1980**, *58*, 1200–1211.

[39] J. P. Perdew, A. Zunger, *Phys. Rev. B* **1981**, *23*, 5048–5079.

[40] A. D. Becke, *Phys. Rev. A* **1988**, *38*, 3098–3100.

[41] C. Lee, W. Yang, R. G. Parr, *Phys. Rev. B* **1988**, *37*, 785–789.

[42] P. M. W. Gill, *Mol. Phys*. **1996**, *89*, 433–445.

[43] C. Adamo, V. Barone, *J. Comput. Chem*. **1998**, *19*, 418–429.

[44] C. Adamo, V. Barone, *J. Chem. Phys*. **1998**, *108*, 664–675.

[45] A. D. Becke, *J. Chem. Phys*. **1996**, *104*, 1040–1046.

[46] A. D. Becke, *J. Chem. Phys*. **1993**, *98*, 5648–5652.

[47] A. D. Becke, *J. Chem. Phys*. **1993**, *98*, 1372–1377.

[48] C. Adamo, V. Barone, *J. Chem. Phys*. **1999**, *110*, 6158–6169.

[49] J. P. Perdew, K. Burke, Y. Wang, *Phys. Rev. B* **1996**, *54*, 16533–16539.

[50] K. Djanashvili, C. Platas-Iglesias, J. A. Peters, *Dalton Trans*. **2008**, 602–607.

[51] a) J. Ciupka, X. Cao-Dolg, J. Wiebke, M. Dolg, *Phys. Chem. Chem. Phys*. **2010**, *12*, 13215–13223; b) B. Kvamme, M. C. F. Wander, A. E. Clark, *Int. J. Quantum Chem*. **2009**, *109*, 2474–2481; c) U. Cosentino, A. Villa, D. Pitea, G. Moro, V. Barone, *J. Phys. Chem. B* **2000**, *104*, 8001–8007.

[52] a) M. Barysz, A. J. Sadlej, *J. Mol. Struct.: THEOCHEM* **2001**, *573*, 181–200; b) M. Reiher, *Theor. Chem. Acc*. **2006**, *116*, 241–252.

[53] D. A. Pantazis, F. Neese, *J. Chem. Theory Comput*. **2009**, *5*, 2229–2238.

[54] M. Orio, D. A. Pantazis, F. Neese, *Photosynth. Res*. **2009**, *102*, 443–453.

[55] N. Rega, M. Cossi, V. Barone, *J. Chem. Phys*. **1996**, *105*, 11060–11067.

[56] J. F. Stanton, J. Gauss, *Adv. Chem. Phys*. **2003**, *125*, 101–146.

[57] A. Montoya, T. N. Truong, A. F. Sarofim, *J. Phys. Chem. A* **2000**, *104*, 6108–6110.

[58] J. Tomasi, B. Mennucci, R. Cammi, *Chem. Rev*. **2005**, *105*, 2999–3093.

[59] J. Reuben, D. Fiat, *J. Chem. Phys*. **1969**, *51*, 4909–4917.

[60] A. V. Arbuznikov, M. Kaupp, V. G. Malkin, R. Reviakine, O. L. Malkina, *Phys. Chem. Chem. Phys*. **2002**, *4*, 5467–5474.

[61] M. Munzarová, M. Kaupp, *J. Phys. Chem. A* **1999**, *103*, 9966–9983.

[62] K. J. de Almeida, Z. Rinkevicious, H. W. Hugosson, A. C. Ferreira, H. Agren, *Chem. Phys*. **2007**, *332*, 176–187.

[63] S. Koβmann, B. Kirchner, F. Neese, *Mol. Phys*. **2007**, *105*, 2049–2071.

[64] a) J. Autschbach, S. Patchkovskii, B. Pritchard, *J. Chem. Theory Comput*. **2011**, *7*, 2175–2188; b) E. Malkin, M. Repisky, S. Komorovsky, P. Mach, O. L. Malkina, V. G. Malkin, *J. Chem. Phys*. **2011**, *134*, 044111.

[65] A. M. Raitsimring, A. V. Astashkin, D. Baute, D. Goldfarb, P. Caravan, *J. Phys. Chem. A* **2004**, *108*, 7318–7323.

[66] J. R. Pliego, J. M. Riveros, *J. Phys. Chem. A* **2001**, *105*, 7241–7247.

[67] a) V. S. Bryantsev, M. S. Diallo, W. A. Goddart III, *J. Phys. Chem. B* **2008**, *112*, 9709–9719; b) V. S. Bryantsev, M. S. Diallo, W. A. Goddart III, *J. Phys. Chem. A* **2009**, *113*, 9559–9567.

[68] C. A. Chang, L. C. Francesconi, M. F. Malley, K. Kumar, J. Z. Gougoutas, M. F. Tweedle, D. W. Lee, L. J. Wilson, *Inorg. Chem*. **1993**, *32*, 3501–3508.

[69] S. W. A. Bligh, A. H. M. S. Chowdhury, M. McPartlin, I. J. Scowen, R. A. Bulman, *Polyhedron* **1995**, *14*, 567–569.

[70] K. Kumar, C. A. Chang, L. C. Francesconi, D. D. Dischino, M. F. Malley, J. Z. Gougoutas, M. F. Tweedle, *Inorg. Chem*. **1994**, *33*, 3567–3575.

[71] H. Gries, H. Miklautz, *Physiol. Chem. Phys. Med. NMR* **1984**, *16*, 105–112.

[72] N. Chatterton, C. Gateau, M. Mazzanti, J. Pecaut, A. Borel, L. Helm, A. E. Merbach, *Dalton Trans*. **2005**, 1129–1135.

[73] A. V. Astashkin, A. M. Raitsimring, P. Caravan, *J. Phys. Chem. A* **2004**, *108*, 1990–2001.

[74] M. Woods, Z. Kovacs, S. Zhang, A. D. Sherry, *Angew. Chem*. **2003**, *115*, 6069–6072; *Angew. Chem. Int. Ed.* **2003**, *42*, 5889–5892.

[75] M. Purgel, Z. Baranyai, A. de Blas, T. Rodríguez-Blas, I. Banyai, C. Platas-Iglesias, I. Toth, *Inorg. Chem*. **2010**, *49*, 4370–4382.

[76] J. Kotek, P. Lebduskova, P. Hermann, L. Vander Elst, R. N. Muller, C. F. G. C. Geraldes, T. Maschmeyer, I. Lukes, J. A. Peters, *Chem. Eur. J*. **2003**, *9*, 5899–5915.

[77] S. Laurent, L. Vander Elst, S. Houzé, N. Guérit, R. N. Muller, *Helv. Chim. Acta* **2000**, *83*, 394–406.

[78] R. De Beer, F. Biesboer, D. Van Ormondt, *Phys. B* **1976**, *83*, 314–317.

[i] MRI: Magnetic resonance imaging.